Nonlinear Dynamics manuscript No.
(will be inserted by the editor)

Unusual dynamics and hidden attractors of the Rabinovich-Fabrikant system

Marius-F. Danca · Nikolay Kuznetsov · Guanrong Chen

the date of receipt and acceptance should be inserted later

Abstract This paper presents some numerical evidence of unusual dynamics and hidden chaotic attractors of the Rabinovich-Fabrikant system, with some insightful descriptions and discussions. From a generalized Hamiltonian energy perspective, the attractors could be analyzed in more details.

Keywords Rabinovich-Fabrikant system · Hidden chaotic attractor · Self-excited attractor · Hamiltonian energy

1 Introduction

The Rabinovich-Fabrikant (RF) system, introduced by Rabinovich and Fabrikant [1] and numerically investigated in [2], was initially established as a physical model describing the stochasticity arising from the modulation instability in a non-equilibrium dissipative medium. However, recently in [2] we revealed that besides the physical properties described in [1], the system presents extremely rich complex dynamics. More significantly, unlike other familiar chaotic systems containing only second-order nonlinearities (such as the Lorenz system), the RF system with third-order nonlinearities presents some unusual dynamics, namely, some complex dynamics that were rarely or never seen from other systems in the past, such as "virtual" saddles in addition to several chaotic attractors with different shapes as well as hidden chaotic attractors and hidden transient chaotic attractors [3]. In fact, common interest in this system is continuously increasing (see e.g. [4–11]).

Marius-F. Danca
Dept. of Mathematics and Computer Science, Avram Iancu University of Cluj-Napoca, Romania
and
Romanian Institute of Science and Technology, Cluj-Napoca, Romania

Nikolay Kuznetsov
Dept. of Applied Cybernetics, Saint-Petersburg State University, Russia
and
Dept. of Mathematical Information Technology, University of Jyväskylä, Finland

Guanrong Chen
Dept. of Electronic Engineering, City University of Hong Kong, Hong Kong, China

The mathematical RF model is described by the following system of ODEs:

$$\begin{aligned} \dot{x}_1 &= x_2\left(x_3 - 1 + x_1^2\right) + ax_1, \\ \dot{x}_2 &= x_1\left(3x_3 + 1 - x_1^2\right) + ax_2, \\ \dot{x}_3 &= -2x_3\left(b + x_1x_2\right), \end{aligned} \tag{1}$$

where a, b are two positive real parameters. The system dynamics depend sensibly on the parameter b but less on a. Therefore, b is typically considered as the bifurcation parameter[1].

Due to the extreme complexity in the dynamics of system (1), a detailed analytical study concerning for example the existence of invariant sets, and of heteroclinic or homoclinic orbits and so on, is very difficult. Therefore, this paper takes a numerical analysis approach, to carefully investigate its new complex dynamics and hidden attractors, further extending the investigations made in [2].

The system presents the following symmetry:

$$T(x_1, x_2, x_3) \to (-x_1, -x_2, x_3), \tag{2}$$

which means that each orbit has its symmetrical ("twin") orbit with respect to the x_3-axis under transformation T, with five equilibria: $X_0^*(0,0,0)$ and

$$\begin{aligned} X_{1,2}^* &\left(\mp\sqrt{\frac{bR_1 + 2b}{4b - 3a}}, \pm\sqrt{b\frac{4b - 3a}{R_1 + 2}}, \frac{aR_1 + R_2}{(4b - 3a)R_1 + 8b - 6a}\right), \\ X_{3,4}^* &\left(\mp\sqrt{\frac{bR_1 - 2b}{3a - 4b}}, \pm\sqrt{b\frac{4b - 3a}{2 - R_1}}, \frac{aR_1 - R_2}{(4b - 3a)R_1 - 8b + 6a}\right), \end{aligned} \tag{3}$$

where $R_1 = \sqrt{3a^2 - 4ab + 4}$ and $R_2 = 4ab^2 - 7a^2b + 3a^3 + 2a$.

As analytically proved in [2], X_0^* is a global attractor for the reduced system on $x_3 = 0$. Also, X_0^* is attracting on the x_3 axis.

The stability of the other four points X_i^*, $i = 1, ..., 4$, cannot be easily evaluated by analytical means. Therefore, in [2] a numerical approach with symbolic computation was used to calculate and analyze the eigenvalues of the system Jacobian at these points.

Extensive numerical tests have led to a conclusion that the available numerical methods for ODEs, such as those implemented with different software packages, or numerical path-following methods, might give unexpectedly different results of the system dynamics even for the same parameter values and initial conditions. On the other hand, contrarily to variable step-size methods, for this system fixed-step-size schemes (such as the standard Runge-Kutta method RK4, and the predictor-corrector LIL method [12] utilized in this paper) give more accurate results. However, as is well known, numerical results depend drastically on the step-size and the initial conditions.

In this paper, it is numerically demonstrated that the RF system presents several unusual "virtual" saddle-like points which apparently exist in relatively large intervals of b values (compared with [2]). Moreover, the existence of hidden attractors is numerically verified and also investigated.

The paper is organized as follows: Section 2 unveils some unusual dynamics of the RF system, Section 3 presents two hidden attractors of the RF system, with conclusion ending the paper in Section 4.

[1] Negative values also generate interesting dynamics, but this case has not much physical meaning and, therefore, is not considered in the present paper.

2 Unusual dynamics of the RF system

The equilibrium X_0^* exists for all values of a, b. The existence of the other equilibria $X_{1,2,3,4}^*$ is determined by the signs of the expressions $4b - 3a$ and $3a^2 - 4ab + 4$ (Fig. 1). The types of stability are presented in Fig. 2.

For equilibria $X_{1,2,3,4}^*$, there exist regions where $X_{1,2,3,4}^*$ do not exist, regions with only equilibria $X_{3,4}^*$ and regions with all equilibria $X_{1,2,3,4}^*$ (Fig. 3). This fact suggests an essential reason for having some unusual dynamical behavior in this system.

This paper reports, for the first time, the existence of some unusual dynamics of the RF system, namely the presence of "virtual" saddles and the dynamics of "double-vortex tornado"-like attractors as well as hidden chaotic attractors.

The parameter b is considered as the bifurcation parameter (see Fig. 3, where the bifurcation diagram of x_3 is plotted for $b \in (0.05, 1.3)$). The parameter a is chosen as $a = 0.1$ because for this value one obtains a large domain of existence of all equilibria (segment AB with $A(0.1, b_1)$ and $B(0.1, b_2)$, where $b_1 = 0.075$, $b_2 = 10.075$, determined by the intersections of $a = 0.1$ and the curves $b = 3/4a$ and $b = (3a^2 + 4)/(4a)$, respectively). For $a > 0.1$ and $b > 11$, the system becomes generally unstable.

As is well known, for calculating numerical solutions of chaotic dynamical systems, the standard double-precision floating-point format over long-time periods is a challenging problem (see e.g. [13]). In this paper, all the numerical results are obtained using the LIL algorithm [12], with step-size $h = 0.0001 - 0.005$, and integration-time interval is $I = [0, T_{max}]$ with $T_{max} = 300 - 500$. The initial conditions $S = (x_{0,1}, x_{0,2}, x_{0,3})$, which have a major impact on the numerical results (especially in finding hidden attractors), are chosen as $x_{0,1}, x_{0,2} \in (-1, 1)$, and $x_{03} \in (0 - 0.2)$.

For $b = 1.8$, in [2] a singularity with interesting behavior was found, which suggests a kind of "virtual" repelling focus saddles, denoted by Y^* (Figs. 4 (c)-(e)). In this case, the dynamics in its neighborhood look like the sketch in Figs. 4 (a), (b), respectively (see also Fig. 4 (c), where the pair of saddles $X_{3,4}^*$ are plotted). However, as can be seen in Figs. 4 (d)-(e), besides the singular case found in [2] (Fig. 4 (b)), this behavior is generic for all values of $b \in (b_1, b_2)$ (see Fig. 4 (d), where for the sake of image clarity only the saddle X_4^* is plotted). It is interesting to observe that for b values lying on the segment AB (situated in the existence domain of all equilibria, Fig. 3), these saddle-like points are connected by smooth curves to the real saddles $X_{3,4}$, appearing as a reversed "replica" of $X_{3,4}$ and being emanated by them.

These saddle-like points exist not only in the existence domain of all equilibria (segment AB), but also in some nonexistence domain of equilibria such as the point $C(b = 11)$ (Fig. 3). While for $b \in AB$, the "virtual"-saddles seem to appear as a consequence of the existence of the real saddles $X_{3,4}^*$, in the nonexistence domain of the equilibria. Wherein, the "virtual"-saddles still appear, even $X_{3,4}^*$ do not exist, which are fairly complex along the x_2-axis (Fig. 3).

Another interesting characteristic of these saddles-like points Y^* is that in the existence domain of the real saddles $X_{3,4}^*$, depending on b, the distance between them and $X_{3,4}^*$ exceeds several times of the underlying attractor size (Figs. 4 (c)-(e)). The unstable direction of $X_{3,4}^*$ acts as a stable direction for Y^* and is the

same for each b. Also, their spinning orientation on $Y^*_{1,2}$ is the same as that on $X_{3,4}$ (Figs. 4 (c) and (d)).

Compared to the case of $b = 0.2715$, where the saddles-like point Y^*_1 (Figs. 9 (a) and (b)) is obtained by starting the numerical integration with initial points in the neighborhoods of X^*_4 (similarly for Y^*_2), in the case of $b = 0.2876$, Y^*_1 (Figs. 8 (a) and (b)) is generated either by starting from the neighborhood of X^*_0 (gray trajectory) or by starting from the neighborhood of X^*_4 (dark-brown trajectory) (similarly for Y^*_2). Because $Y^*_{1,2}$ are generated from some points in the vicinities of unstable equilibria X^*_0 and $X_{3,4}$, and due to the divergence to infinity indicated by the numerical tests, these points can be classified as unbounded self-excited attractors.

For values of $b < 0.075$ (point $D(b = 0.05)$, Fig. 3) and $h = 0.005$, these saddle-like points disappear and transform into stable "double-vortex tornado"-like cycles (Fig. 5 (a)). Plane phase plots (Figs. 5 (b)-(d)), time series, the inset D (Fig. 5 (e)), the power spectrum (Figs. 5 (f)) and Poincaré sections (Figs. 5 (g)-(i)), all together show a possible quasiperiodic motion. It is noted that these attractors exist only in the regions where equilibria $X^*_{3,4}$ exist.

As mentioned before, spectacular phenomena appear depending on the h size. In fact, for a smaller integration step-size, $h = 0.0005$, the vortexes still exist, but with a larger size along the x_3-axis, together with an enlarged base (see the phase plot in Fig. 6 (a) and the time series with inset D_1 in Fig. 6 (b)). While for $h = 0.0001$, the vortices disappear but their base seems to transform into a stable periodic motion (see the phase plot with and without transients in Fig. 6 (c), and the time series and the inset D_2 in Fig. 6 (d)). Apparently, this quasiperiodic motion with variable sizes along the x_3-axis is due to a long numerical step-size. However, the considered variable-step numerical schemes fail to integrate the system in this case. Also, as Fig. 6 shows, this phenomenon persists for the numerical scheme with even smaller step-sizes.

Possibly because of numerical errors, the life-time of these attractors is relatively short and, consequently, the underlying trajectories might diverge (see e.g. Fig. 4).

3 Hidden chaotic attractors of the RF system

From a computational perspective, it is natural to suggest the following classification of attractors[2], which is based on the connection of their basins of attraction with equilibria in the phase space.

The notion of self-excited oscillations (or self-oscillations) can be traced back to the works of Barkhausen and Andoronov where it was used to describe the generation and maintenance of a periodic motion in mechanical and electrical

[2] Since from a computational perspective it is essential that an attractor can be found numerically, we adopt the following definition: A closed bounded invariant set K is called an attractor if there exists an open ε-neighborhood of K: $K_\varepsilon \supset K$, such that for all initial points from K_ε (except a zero-measure set) the corresponding trajectories tend to K as $t \to \infty$. This gives a hope that the attractor can be revealed numerically, despite possible computational errors (we do not consider the computational difficulties caused by the shape of the basin of attraction, e.g. Wada and riddled basins). Note that a semistable trajectory on the plane has a basin of attraction with a positive measure, but can hardly be computed by the usual methods because of the implemented step in the computational procedure (see, e.g. [14–16]).

models by a power source that lacks corresponding periodicity (e.g., stable limit cycle in van der Pol oscillator). Generalization of this notion for attractors of dynamical systems was introduced to describe the existence of the corresponding transient process from a small vicinity of unstable equilibria to an attractor (e.g. Lorenz attractor, which is self-excited with respect to the zero equilibrium). If there is no such a transient process for an attractor, it is called a hidden attractor. This notion was recently introduced in connection with the discovery of a hidden Chua attractor [17,18], detailed as follows.

Definition 1 [17–20] An attractor is called a self-excited attractor if its basin of attraction intersects with any arbitrarily small open neighborhood of a stationary state (an equilibrium); otherwise, it is called a hidden attractor.

Self-excited attractors can be numerically visualized by a standard computational procedure, in which after a transient process a trajectory starting from a point of in a neighborhood of an unstable equilibrium is attracted to the attractor. In contrast, the basin of attraction for a hidden attractor is not connected with any equilibrium and, thus, for the numerical localization of a hidden attractor it is necessary to develop a special analytical-numerical procedure, in which an initial point is chosen from the basin of attraction. For example, hidden attractors can be in systems with no-equilibria or in a multistable system with only stable equilibrium. At the same time, the coexisting self-excited attractors in multistable systems (see, e.g., various examples of multistable engineering systems in [15,21], and recent physical examples in [22]) can be found following a standard computational procedure, whereas there is no regular way to predict the existence or coexistence of hidden attractors in a system [22,23] (see also [24–27]).

Among the complicated and unusual dynamics analyzed in Section 2 (such as multistability, coexistence of chaotic attractors and stable cycles), and heteroclinic orbits connecting different kinds of attractors [2], the RF system also presents several chaotic attractors with different shapes (Fig. 7). Among these attractors, it is found that two attractors, corresponding to $b = 0.2876$ and $b = 0.2715$ respectively, are hidden. The others are self-excited attractors: there does not seem to exist small neighborhoods around the unstable equilibria such that all trajectories starting from inside these neighborhoods tend to infinity or are attracted to stable equilibria.

Now, consider the chaotic attractor H_1 (Fig. 7 (b)) corresponding to $a = 0.1$ and $b = 0.2876$. In order to verify that this attractor is hidden, Definition 1 is used to show that its attraction basin does not intersect with any small neighborhoods of unstable equilibria. For this purpose, initial points are chosen from inside δ-vicinities of unstable equilibria (here $\delta = 0.05$) and the system is integrated to see if the obtained trajectories are attracted by the chaotic attractor. For all unstable equilibria, this procedure is repeated for several times (with 100 random choices of different initial points).

For the chosen parameters, the equilibrium X_0^* is a repelling focus-saddle, equilibria $X_{1,2}^*$ are stable focus-nodes and equilibria $X_{3,4}^*$ are attracting focus saddles (see [2] and Table 2).

First, check the δ-vicinity of the equilibrium X_0^*, $V_{X_0^*}$. As analytically proved in [2], for $x_3 = 0$, all trajectories starting from $V_{X_0^*}$ diverge to infinity and therefore are not considered in these numerical simulations. The origin is globally asymptotically unstable. For $x_3 > 0$ (as required by the physical system structure [1]),

numerical simulations show that all trajectories starting from $V_{X_0^*}$ either tend to ∞, via $Y_{1,2}^*$ (Figs. 8 (a)) along the grey and black trajectories (Figs. 8 (b) and (d)) after scrolling out along the unstable equilibria $X_{3,4}^*$, or tend to $X_{1,2}^*$ along the stable $1D$ manifold of $X_{1,2}^*$ (dotted red and blue trajectories in Figs. 8 (b) and (d)), as $t \to \infty$. The hidden attractor (grey line in Fig. 8) is obtained with initial condition $(1.8, 1.1, 0.1)$.

Next, consider equilibria $X_{3,4}$ which, due to the symmetry (2), behave similarly. Fig. 8 (c), for the sake of clarity, presents only 25 trajectories starting from the vicinity of X_4^*. It reveals that the trajectories either tend to infinity by scrolling out around the unstable $1D$ manifold of X_4^* (dark-brown trajectory) or tend to the equilibrium X_1^* along the stable $1D$ manifold of X_1^* (blue trajectory). Similarly, the simplified case of only two representative trajectories starting from $V_{X_3^*}$ (Fig. 8 (e)) indicates that all trajectories starting from inside the δ-neighborhood of X_3^* tend either to infinity (black trajectory) or to X_2^* (dotted red trajectory).

Note that very large vicinities might lead to intersections of the neighborhoods of the equilibria with the basin of attraction of the considered chaotic attractor.

Summarizing, all trajectories starting from the neighborhoods of unstable equilibria $X_{0,3,4}$, either tend to infinity, or are attracted to the stable equilibria $X_{1,2}^*$ but not to the chaotic attractor.

Another hidden chaotic attractor, H_2, corresponds to $a = 0.1$ and $b = 0.2715$ (Fig. 9). The difference of this setting from the case of $b = 0.2876$ lies in that the divergent trajectories starting from $V_{X_0^*}$ are no longer attracted by the "virtual" saddles (Figs. 9 (a), (b)). In this case, the hidden attractor H_2 is obtained from the initial point $(0.1, 0.1, 0.1)$. As known for hidden attractors, initial points form a dense set (attraction basin) with a fractal structure. Therefore, one can find several other points in neighborhoods of considered initial points, which lead the orbits to $H_{1,2}$.

4 Energy-based analysis of RF system attractors

While the classical use of some quadratic positive-definite energy functions of the state variables, fail to uncover some particular characteristics of the dynamics dynamics, in [33] it is presented a procedure to find a specific (generalized Hamiltonian) energy function $\mathcal{H}$ to describe the energy of a considered chaotic system (see also [30–32]).

The fundamental Helmholtz theorem of vector calculus [34–36] states that a vector field can be decomposed as the sum of an irrotational part (curl-free) and a solenoidal part (divergence-free). Thus, the right-hand side smooth function f in (1) can be written as follows: $f = f_c + f_d$, where f_d carries the divergence of f (curl-free component: $curl(f_d) = 0$) and f_c accounts of for the whole rotor of f (divergence-free: $div(f_c) = 0$)

$$f_c(x) = \begin{pmatrix} x_2(x_3 - 1 + x_1^2) \\ x_1(3x_3 + 1 - x_1^2) \\ -2x_3x_1x_2 \end{pmatrix}, \quad f_d(x) = \begin{pmatrix} ax_1 \\ ax_2 \\ -2bx_3 \end{pmatrix}.$$

In practice, f_d can be determined considering all the terms in f that contribute to its divergence, while the other terms represent f_c.

For the particular case $A = B = 1$, the energy function $\mathcal{H}$ becomes (see (A.1) in Appendix)

$$\mathcal{H}(x) = x_1^2(x_3 + 1) + x_1^2 + x_2^2 + \frac{x_3^2}{2} + 3x_3, \tag{4}$$

and the derivative of $\mathcal{H}$ (relation (A.3) in Appendix) is

$$\dot{\mathcal{H}}(x) = 2\left((a-b)x_1^2x_3 - bx_3^2 + a(x_1^2 + x_2^2) - 3bx_3\right). \tag{5}$$

The isosurface considered in arbitrary units, $\mathcal{H} = 5$, is plotted in Figs. 10 (a) and (b) for the hidden attractors. While the isosurfaces are identical for all attractors (see (4)), each attractor has different conservative trajectories, obtained by solving the equation $\dot{x} = f_c(x)$ (curves $C_{1,2}$ in Fig. 10 (a) for hidden attractor H_1 and C (Fig. 10 (b)) for hidden attractor H_2, respectively.

Compared with other classical chaotic systems like Lorenz, Chen, Rössler or Chua system, the energy $\mathcal{H}$ of the RF system does not depend on the system parameters, a and b. Also, since for all attractors of the RF system, $x_3 > 0$, $\mathcal{H}$ is positive definite (compare [33]).

In order to compare the attractors in terms of the Hamiltonian energy, in Figs. 11 the time series of x_3, $\mathcal{H}$ and $\dot{\mathcal{H}}$ are plotted for the most representative cases considered here: $b = 0.05$ (Fig. 11 (a)), $b = 1.8$ (Fig. 11 (b)), $b = 0.2876$ (Fig. 11 (c)) and $b = 0.2715$ (Fig. 11 (d)).

As can be seen, the energy $\mathcal{H}$ and its rate of change $\dot{\mathcal{H}}$ for the cases of $b = 0.05$ and $b = 1.8$ are much larger than that for the cases of $b = 0.2876$ and $b = 0.2715$. Even the shapes of the hidden attractors H_1 and H_2 in the phase space resemble, for which the time series of $\mathcal{H}$ and $\dot{\mathcal{H}}$ reveal several differences. On the other hand, both attractors present the same evolution: when the trajectory reaches extremum points (e.g. the points m and M in Fig. 11 (c) for $b = 0.2876$), the energy has a medium value but not an extreme value, as expected.

The equation (5) for $\dot{\mathcal{H}}$ shows that the system could be dissipative since the energy can either decrease or increase depending on the values of x_3 which, for the RF system, is always positive. On the other hand, $div(f) = 2(a - b) < 0$ for the values of $b > a$: $b \in \{0.2715, 0.2876, 0.75, 0.98, 1.215, 1.8, 1.9, 5.5, 8, 11, -0.1\}$, is dissipative. However, for the b values corresponding to saddles-like points, namely $b \in \{0.75, 0.98, 1.8, 1.9, 5.5, 8, 11\}$ (see points Y^*, Fig. 4), the system presents trajectories escaping finally to infinity, somewhat in contradiction with the dissipativity. Also, for $b = 0.05$, $div(f) > 0$ ($b < a = 0.1$) and, for a finite time, the trajectory seems to follow a stable cycle, after which it tends to infinity. However, for a finite time interval, compared to the case of saddles-like points, in the case of $b = 0.05$ the energy required by the cycle oscillates but remains bounded (Fig. 11 (a)), while for the case of saddle-like points, it keeps increasing monotonically (Fig. 11 (b)). As mentioned in Section 2, numerical errors could play a significant role here, so further studies are needed in future research.

Acknowledgements We thank Michal Fečkan for his help. NK is supported by the Russian Science Foundation 14-21-00041, GC by the Hong Kong Research Grants Council under the GRF Grant CityU 11208515.

5 Conclusions

In this paper, it is shown via extensive and careful numerical investigations, helped by the Hamiltonian energy concept, that compared to many other classical nonlinear systems, the RF system presents unusual dynamics, which appear within a large interval of the key parameter b. Also, hidden chaotic attractors have been identified. Contrarily to the common belief that numerical results should be independent of the numerical methods and the integration step-size if the methods and steps are used properly, the results obtained in the case of the RF system clearly depend on the utilized numerical integration method and the step-size; otherwise, some intrinsic interesting dynamical behavior won't be able to reveal. It is important to note that the saddle-like points may relate to the so-called "bifurcation delay" along the invariant line x_3 [28,29]. Therefore, future work on this issue may clarify the appearance of these points.

Appendix

To calculate the Hamilton energy $\mathcal{H}$, one needs to solve the linear PDE (see e.g. [30])

$$\nabla \mathcal{H}^T f_c(x) = 0,$$

which leads to the system

$$\frac{dx_1}{x_2(x_3 - 1 + x_1^2)} = \frac{dx_2}{x_1(3x_3 + 1 - x_1^2)} = \frac{dx_3}{-2x_3x_1x_2}.$$

Two solutions are

$$\mathcal{H}_1(x) = x_1^2 x_3 - x_3 + \frac{x_3^2}{2} \quad \text{and} \quad \mathcal{H}_2(x) = x_1^2 + x_2^2 + 4x_3,$$

and the general form of the Hamiltonian energy for the RF system is

$$\mathcal{H}(x) = h(\mathcal{H}_1(x), \mathcal{H}_2(x)), \tag{A.1}$$

with some linear function $h(y_1, y_2) = Ay_1 + By_2$, $A, B \in \mathbb{R}$.

The derivative of $\mathcal{H}(x)$ according to [33, Eq. (8)] is given by

$$\begin{aligned} \dot{\mathcal{H}}(x) &= \nabla \mathcal{H}^T f_d(x) \\ &= h_{y_1}(\mathcal{H}_1(x), \mathcal{H}_2(x)) \nabla \mathcal{H}_1^T f_d(x) + h_{y_2}(\mathcal{H}_1(x), \mathcal{H}_2(x)) \nabla \mathcal{H}_2^T f_d(x). \end{aligned} \tag{A.2}$$

Considering the form (4), it follows from (A.2) that

$$\dot{\mathcal{H}}(x) = 2A\left((a-b)x_1^2 x_3 + bx_3 - bx_3^2\right) + 2B\left(a(x_1^2 + x_2^2) - 4bx_3\right). \tag{A.3}$$

References

1. Rabinovich, M.I., Fabrikant, A.L.: Stochastic self-modulation of waves in nonequilibrium media. J.E.T.P. (Sov.) **77**, 617-629 (1979)
2. Danca, M.-F., Feckan, M., Kuznetsov, N., Chen, G.: Looking more closely to the Rabinovich-Fabrikant system. Int. J. Bifurc. Chaos, **26**, 1650038 (2015)
3. Danca, M.-F.: Hidden transient chaotic attractors of Rabinovich-Fabrikant system. Nonlinear Dyn. **86**, 1263-1270 (2016)
4. Liu, Y., Yang, Q., Pang, G.: A hyperchaotic system from the Rabinovich system. J. Comput Appl. Math. **234**, 101-113 (2010)
5. Zhang, C.-X., Yu, S.-M., Zhang, Y.: Design and realization of multi-wing chaotic attractors via switching control. Int. J. Mod. Phys. B **25**, 2183 (2011)
6. Motsa, S.S., Dlamini, P.G., Khumalo, M.: Solving Hyperchaotic Systems Using the Spectral Relaxation Method. Abstr. Appl. Anal. **2012**, 203461 (2012)
7. Agrawal, S.K., Srivastava, M., Das, S.: Synchronization between fractional-order Ravinovich-Fabrikant and Lotka-Volterra systems. Nonlinear Dyn. **69**, 3361-3372 (2014)
8. Chairez, I.: Multiple DNN identifier for uncertain nonlinear systems based on Takagi-Sugeno inference. Fuzzy Set. Syst. **237**, 118-135 (2014)
9. Umoh, E.A. Edited by: Achumba, I.E; Diala, U.H.; Atimati, IEEE International Conference on Emerging and Sustainable Technologies for Power and ICT in a Developing Society (NIGERCON) Owerri, Date: Nov 14-16, 217-222 (2013)
10. Serrano-Guerrero, H., Cruz-Hernández, C., López-Gutiérrez, R.M., Cardoza-Avendaño, L., Chávez-Pérez, R.A.: Chaotic Synchronization in Nearest-Neighbor Coupled Networks of 3D CNNs. J. Appl. Res. Technol. **11**, 26-41 (2013)
11. Srivastava, M., Agrawal, S.K., Vishal, K., Das S.: Chaos control of fractional order RabinovichFabrikant system and synchronization between chaotic and chaos controlled fractional order Rabinovich-Fabrikant system. Appl. Math. Model. **38**, 3361 (2014)
12. Danca, M.-F.: A multistep algorithm for ODEs, Dynamics of Continuous. Discrete & Impulsive Systems, B **13**, 803-821 (2006)
13. Sarra, S.A., Meador, C.: On the numerical solution of chaotic dynamical systems using extend precision floating point arithmetic and very high order numerical methods. Nonlinear Analysis: Modelling and Control, **16**, 340-352 (2011)
14. Kuznetsov, N.V., Leonov, G.A., Yuldashev, M.V., Yuldashev, R.V.: Nonlinear analysis of classical phase-locked loops in signal's phase space, IFAC Proceedings Volumes (IFAC-PapersOnline) **19**, 8253 (2014)
15. Kuznetsov, N.V.: Hidden attractors in fundamental problems and engineering models. A short survey, AETA 2015: Recent Advances in Electrical Engineering and Related Sciences, Lecture Notes in Electrical Engineering, **371**, 13-25 (2016)
16. Bianchi, G., Kuznetsov, N.V., Leonov, G.A., Yuldashev, M.V., Yuldashev, R.V.: 7th International Congress on Ultra Modern Telecommunications and Control Systems and Workshops (ICUMT), Limitations of PLL simulation: hidden oscillations in MATLAB and SPICE, 79-84 (2015) http://arxiv.org/pdf/1506.02484.pdf, http://www.mathworks.com/matlabcentral/fileexchange/52419-hidden-oscillations-in-pll.
17. Leonov, G.A., Kuznetsov, N.V., Vagaitsev, V.I.: Localization of hidden Chua's attractors. Physics Letters A **375**, 2230-2233 (2011)
18. Leonov, G.A., Kuznetsov, N.V., Vagaitsev, V.I.: Hidden attractor in smooth Chua systems. Physica D: Nonlinear Phenomena **241**, 1482-1486 (2012)
19. Leonov, G.A., Kuznetsov, N.V.: Hidden attractors in dynamical systems: From hidden oscillations in Hilbert-Kolmogorov, Aizerman, and Kalman problems to hidden chaotic attractors in Chua circuits. Int. J. Bifurc. Chaos **23**, 1330002 (2013)
20. Leonov, G., Kuznetsov, N., Mokaev, T.: Homoclinic orbits, and self-excited and hidden attractors in a Lorenz-like system describing convective fluid motion. Eur. Phys. J. Special Topics **224**, 1421-1458 (2015)
21. Andronov, A.A., Vitt, E.A., Khaikin, S.E.: Theory of Oscillators (in Russian). ONTI NKTP SSSR (1937) (English transl. 1966, Pergamon Press).
22. Pisarchik, A., Feudel, U.: Control of multistability, Physics Reports **540**, 167-218 (2014)
23. Dudkowski, D., Jafari, S., Kapitaniak, T., Kuznetsov, N.V., Leonov, G.A., Prasad, A.: Hidden attractors in dynamical systems. Physics Reports **637**, 1-50 (2016)
24. Wei, Z., Pham, V.T., Kapitaniak, T., Wang, Z.: Bifurcation analysis and circuit realization for multiple-delayed Wang-Chen system with hidden chaotic attractors. Nonlinear Dynamics **85**(3), 16351650 (2016)

25. Akgul, A., Calgan, H., Koyuncu, I., Pehlivan, I., Istanbullu, A.: Chaos-based engineering applications with a 3D chaotic system without equilibrium points. Nonlinear Dynamics **84**(2) 481-495 (2016)
26. Chaudhuria, U., Prasad, A.: Complicated basins and the phenomenon of amplitude death in coupled hidden attractors. Phys. Lett. A, **378**(9), 713-718 (2014)
27. Akgul, A., Pehlivan, I.: A new three-dimensional chaotic system without equilibrium points, its dynamical analyses and electronic circuit application. Technical Gazette, **23**(1), 209-214 (2016)
28. Benoît, E.: Bifurcation delay - the case of the sequence: stable focus - unstable focus - unstable node. Discr. Cont. Dyn. Sys. - Series S, arXiv:0901.2883 [math.DS]
29. Baer, S.M., Erneux, T., Rinzel, J.: The slow passage through a Hopf bifurcation: Delay, memory effects, and resonance, SIAM Journal on Applied Mathematics, **49**, 55-71 (1989)
30. Li, F. Yao, C.: The infinite-scroll attractor and energy transition in chaotic circuit. Nonlinear Dyn. **84**, 2305–2315 (2016)
31. Torrealdea, F.J., d'Anjou A., Graña, M.: Energy aspects of the synchronization of model neurons. Phys. Rev. **74**, 011905 (2006)
32. Song, X.L., Jin W.Y., Ma, J.: Energy dependence on the electric activities of a neuron. Chin. Phys. B **24** 128710 (2015)
33. Sarasola, C., Torrealdea, F.J., dAnjou, A., Moujahid, A., Graña, M.: Energy balance in feedback synchronization of chaotic systems, Physical Review E 69, 011606 (2004)
34. Panofsky, W.K.H., Phillips, M.: Classical Electricity and Magnetism, Addison-Wesley Series in Physics Addison-Wesley, Reading, MA, 1962, pp. 27
35. Donald, K.H.: Helmholtzs theorem revisited. Am. J. Phys. **54**, 552 (1986)
36. Rohrlich, F.: The validity of the Helmholtz theorem, Am. J. Phys. **72**, 412-413 (2004)

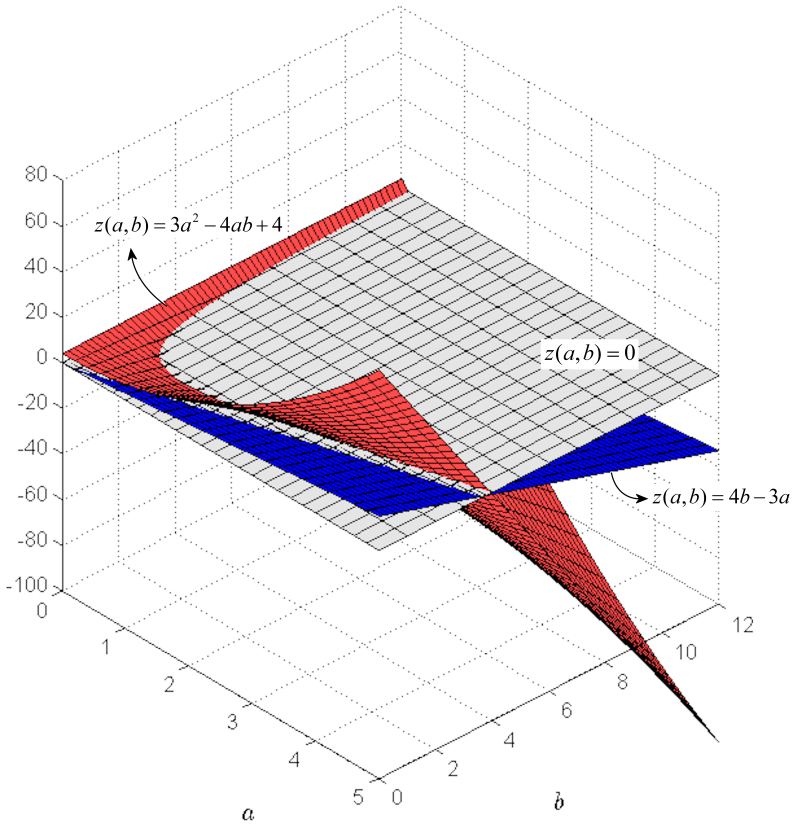

Fig. 1 Surfaces $z(a,b)=4b-3a$ and $z(a,b)=3a^2-4ab+4$.

	$b\in(0.13,1.05)$	$b\in(1.05,1.67)$	$b\in(1.67,2)$
X_0^*	repelling focus	repelling focus	repelling focus
$X_{1,2}^*$	stable focus	repelling focus	stable focus
$X_{3,4}^*$	attracting focus	attracting focus	attracting focus

Fig. 2 Equilibria X_0^* and $X_{1,2,3,4}^*$.

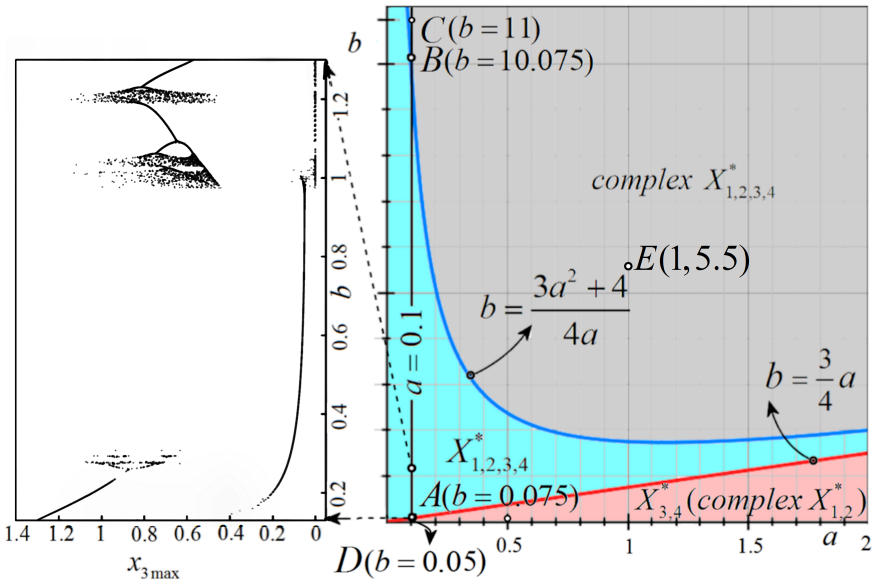

Fig. 3 Existence domain of equilibria in the parameter plane (a, b) and the bifurcation diagram for $b \in (0.075, 1.3)$.

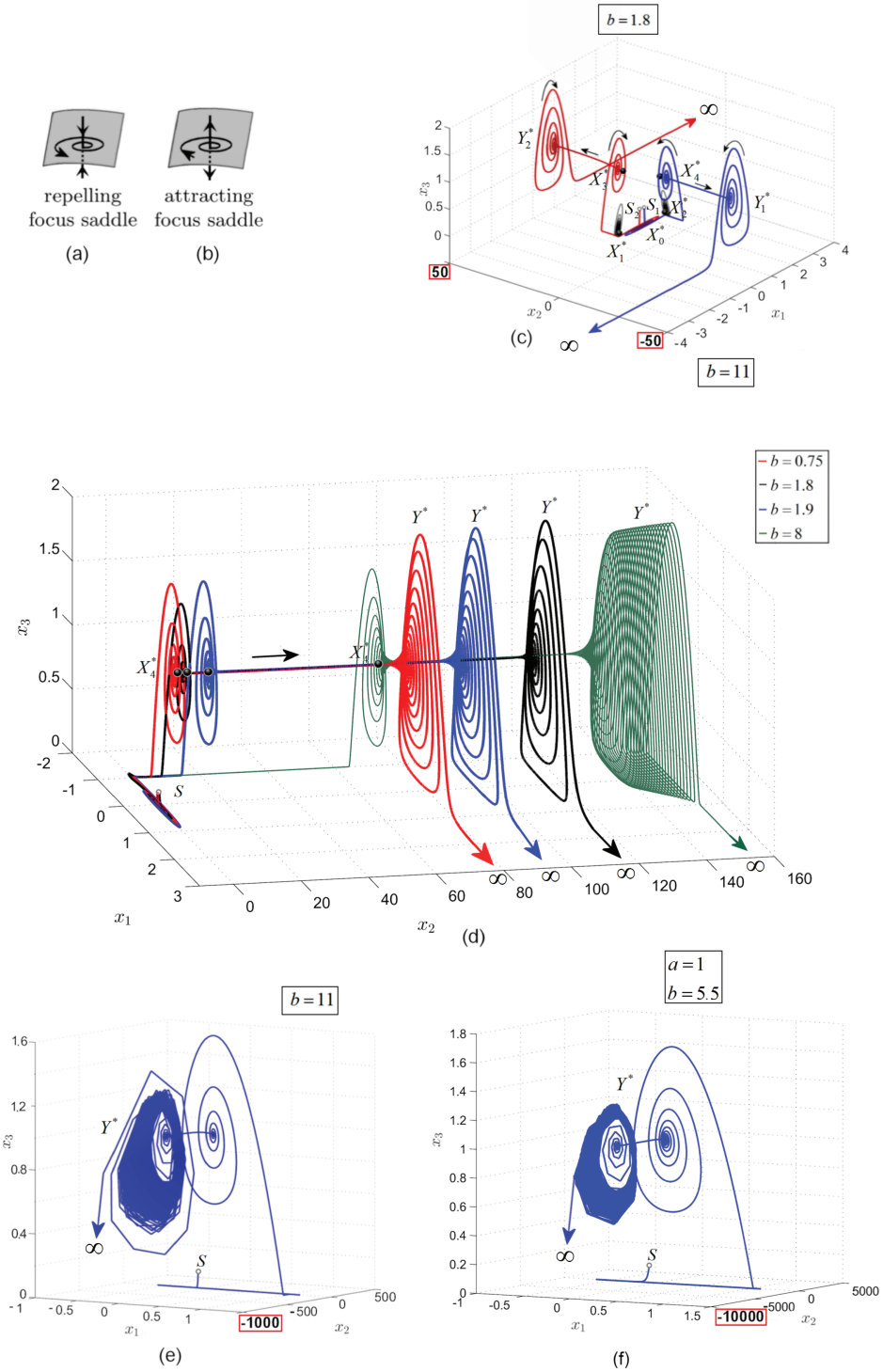

Fig. 4 (a), (b) Repelling and attracting focuses (sketch). (c) "Virtual" saddle for $b = 1.8$ [2]; $S_{1,2}$ are initial conditions. (d) "Virtual" saddles for $b = 0.75, 1.8, 1.9, 8$. (e) "Virtual" saddle for $b = 11$ (equilibria $X^*_{3,4}$ does not exist). (f) "Virtual" saddle for $a = 1$ and $b = 5.5$ (equilibria $X^*_{3,4}$ does not exist).

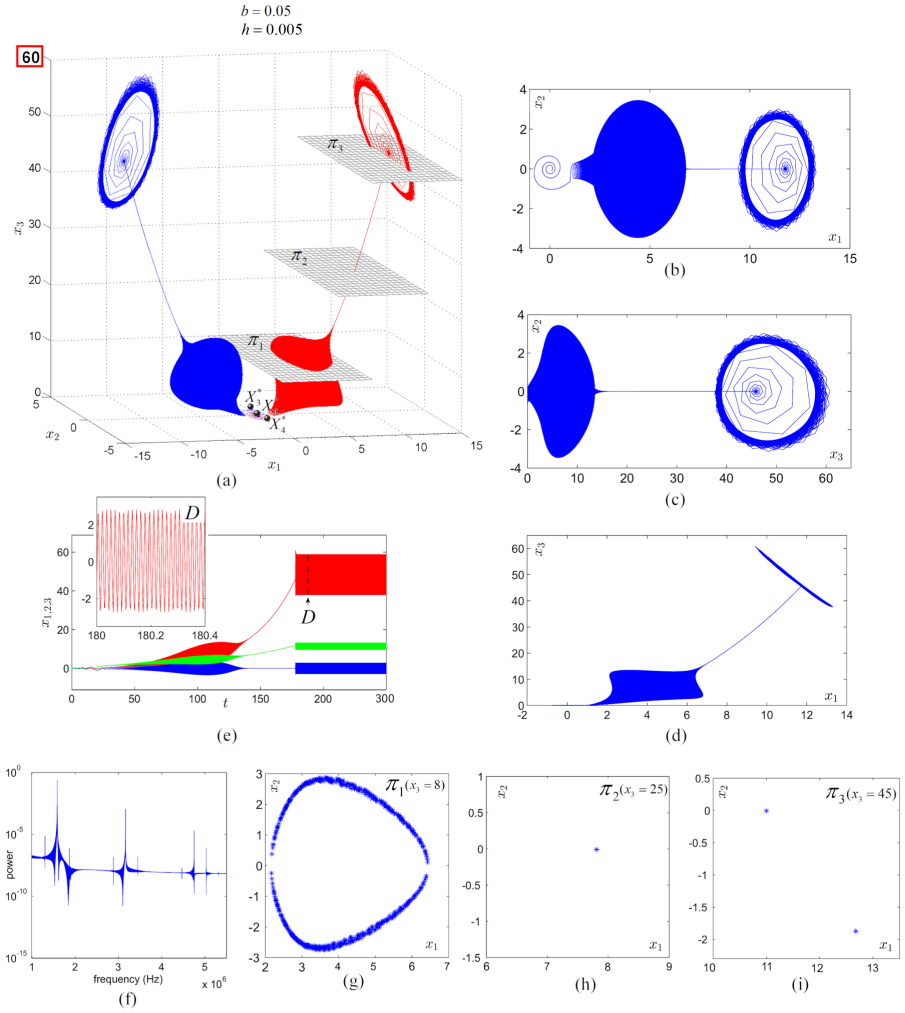

Fig. 5 (a) Double-vortex-like "tornados" for $b = 0.05$ and $h = 0.005$. (b)-(d) Planar phase plots. (e) Time series and inset D. (f) Power spectrum. (g)-(i) Poincaré sections.

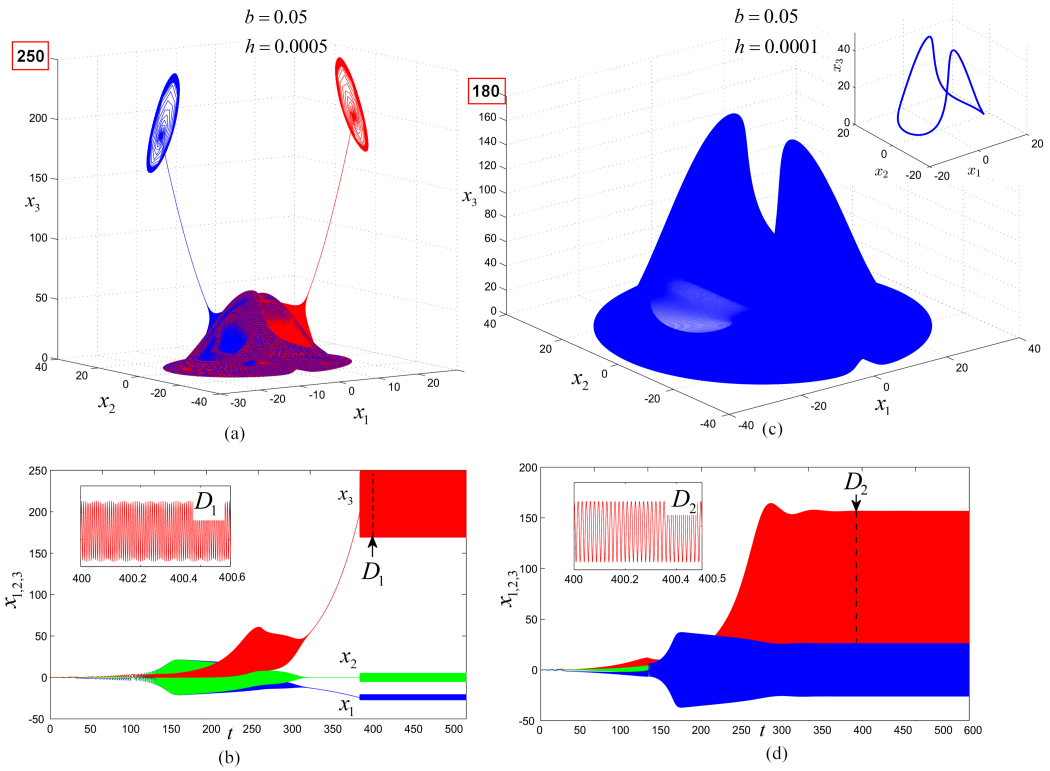

Fig. 6 (a) Double-vortex-like "tornados" for $b = 0.05$ and $h = 0.0005$. (b) Time series and inset D_1. (c) Stable cycles with and without transients for $b = 0.05$ and $h = 0.0001$, respectively. (d) Time series and inset D_2.

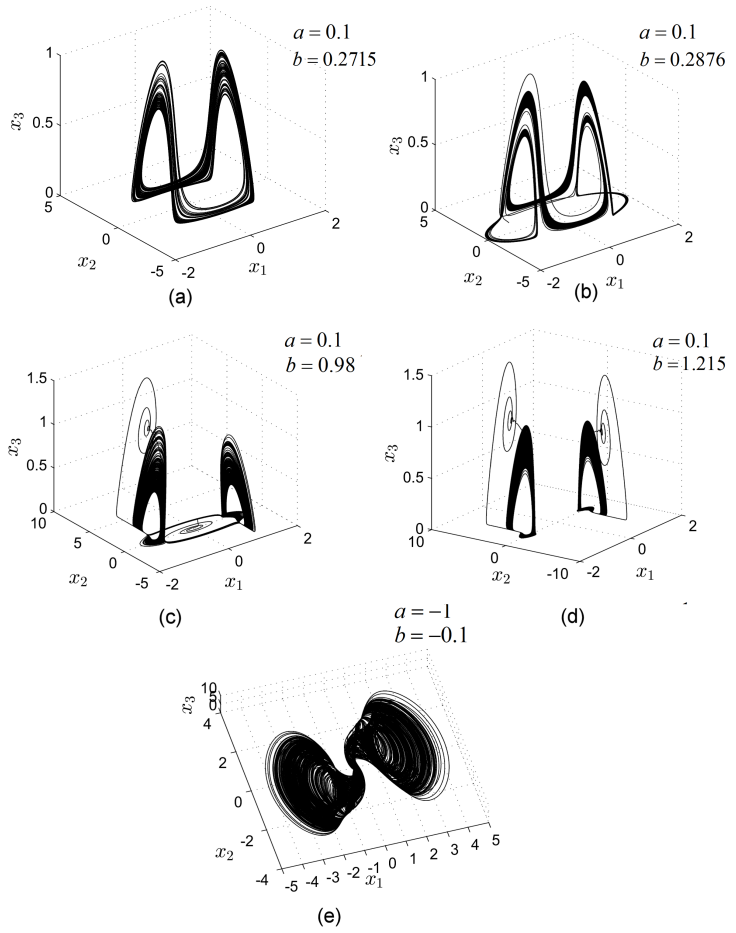

Fig. 7 Chaotic attractors: (a), (b) Hidden chaotic attractors. (c)-(e) Self-excited chaotic attractors.

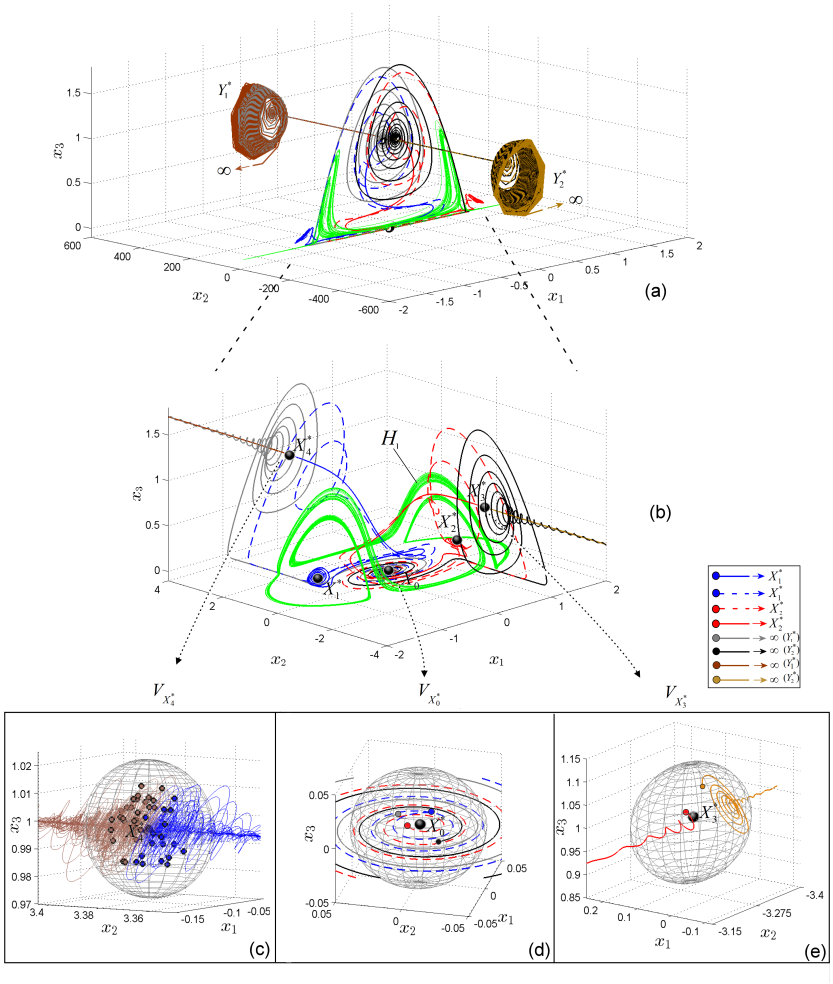

Fig. 8 (a) Hidden chaotic attractor (green) for $b = 0.2876$ and related "virtual" saddles $Y^*_{1,2}$. (a) Detail of the hidden chaotic attractors, trajectories diverging to infinity (via $Y^*_{1,2}$) and trajectories attracted by the stable equilibria $X^*_{1,2}$. (c) Trajectories starting from the δ-vicinity of X^*_4 either are attracted by the equilibrium X^*_1 (blue), or diverge to infinity via Y^*_1 (dark brawn) (50 trajectories). (d) Trajectories starting from the δ-vicinity of X^*_0, either diverge to infinity via $Y^*_{1,2}$ (black and grey trajectories), or tend to $X^*_{1,2}$ (dotted red and blue trajectories) (4 representative trajectories). (e) Trajectories starting form the δ-vicinity of X^*_3 either tend to X^*_2 (red), or diverge to infinity (brawn) via Y^*_2 (two representative trajectories).

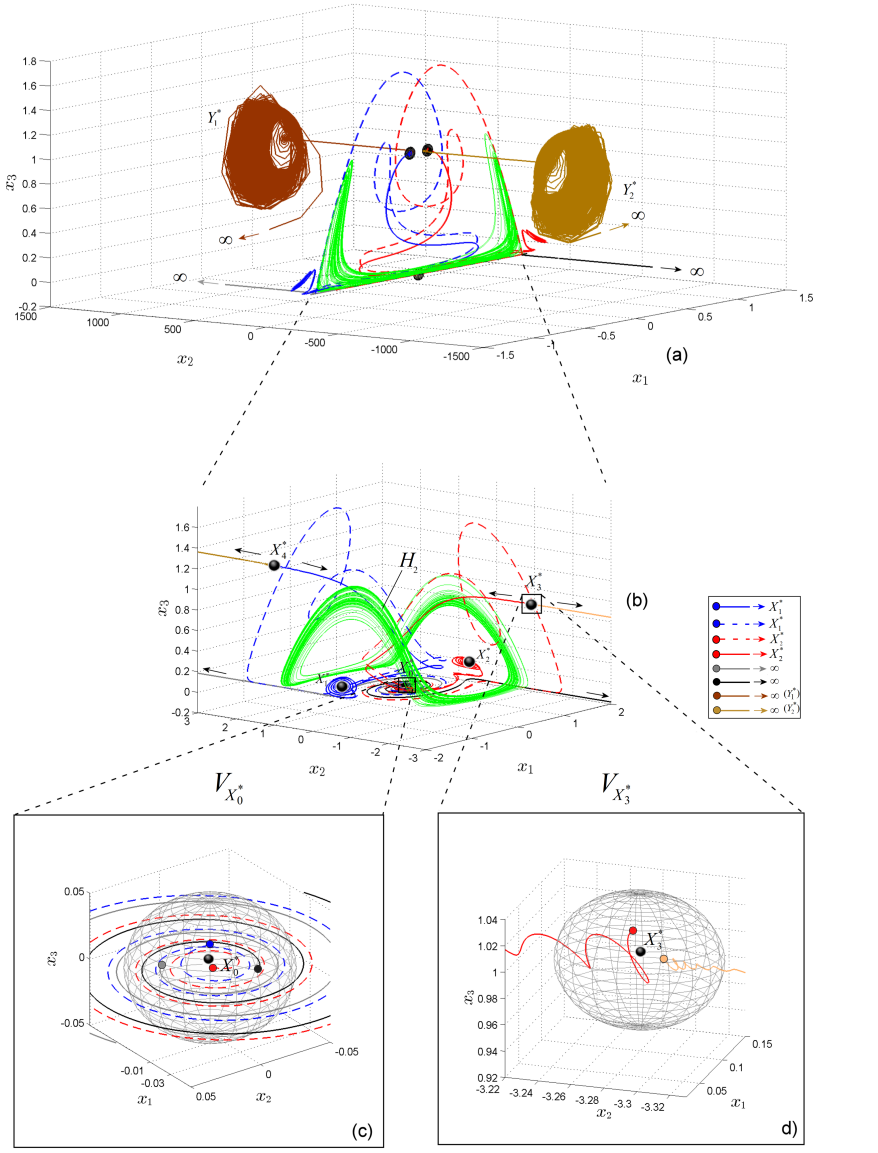

Fig. 9 (a) Hidden chaotic attractor (green) for $b = 0.2715$ and the "virtual" saddles $Y^*_{1,2}$. (b) Detail of the hidden chaotic attractors, trajectories diverging to infinity (via $Y^*_{1,2}$) and trajectories attracted by equilibria $X^*_{1,2}$. (c) Trajectories starting from the δ-vicinity of X^*_0, either diverge to infinity via $Y^*_{1,2}$ (black and grey trajectories), or tend to $X^*_{1,2}$ (dotted red and blue trajectories) (4 representative trajectories). (d) Trajectories starting form the δ-vicinity of X^*_3 either tend to X^*_2 (red), or diverges to infinity via Y^*_2 (brawn) (two representative trajectories).

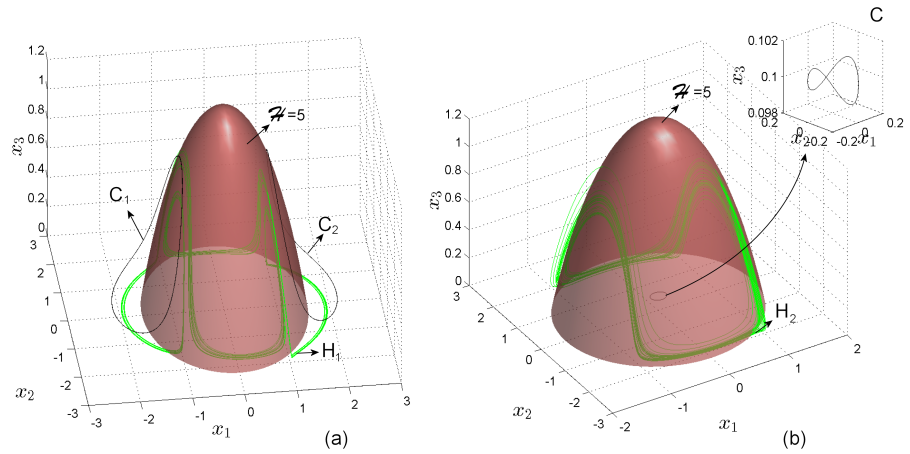

Fig. 10 Isosurface $\mathcal{H} = 5$ (red), hidden attractors $H_{1,2}$ (green) and conservative trajectories (black). (a) Case $b = 0.2876$. (b) case $b = 0.2715$.

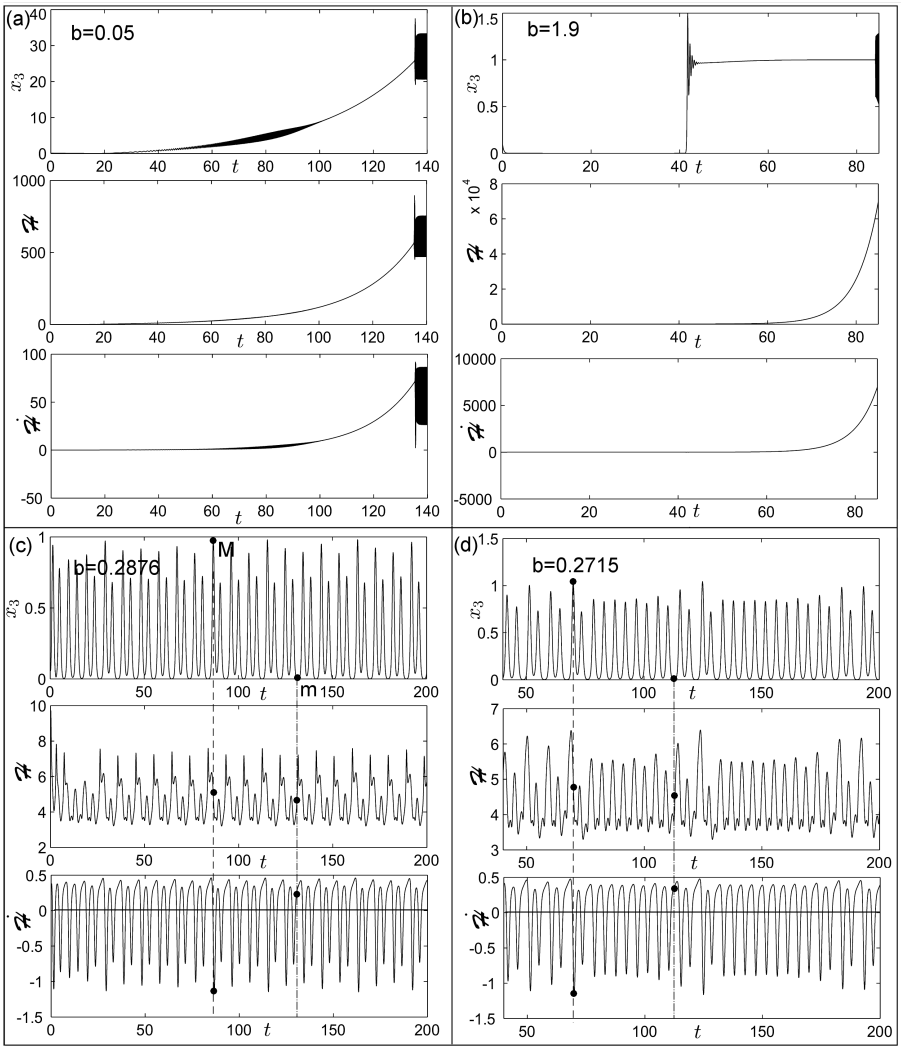

Fig. 11 Time series of variable x_3, $\mathcal{H}$ energy and derivative of $\dot{\mathcal{H}}$. (a) $b = 0.05$. (b) $b = 1.9$. (c) $b = 0.2876$. (d) $b = 0.2715$.